JOC The Journal of Organic Chemistry

Article

pubs.acs.org/joc

Conformational Change with Steric Interactions Affects the Inner Sphere Component of Concerted Proton–Electron Transfer in a Pyridyl-Appended Radical Cation System

Evan A. Welker,[†] Brittney L. Tiley,[†] Crina M. Sasaran,[†] Matthew A. Zuchero,[†] Wing-Sze Tong,[†] Melissa J. Vettleson,[†] Robert A. Richards,[†] Jonathan J. Geruntho,[†] Stefan Stoll,[‡] Jeffrey P. Wolbach,*[,¶] and Ian J. Rhile*[,†]

[†]Department of Chemistry and Biochemistry, Albright College, Reading, Pennsylvania 19610-5234, United States

[‡]Department of Chemistry, University of Washington, Seattle, Washington 98195-1700, United States

[¶]Eurofins Lancaster Laboratories, Lancaster, Pennsylvania 17601, United States

Supporting Information

ABSTRACT: Proton-coupled electron transfer (PCET) model systems combine one-electron oxidants and bases to generate net hydrogen atom acceptors. We have generated two persistent pyridyl-appended radical cations: 10-(pyrid-2-yl)-10*H*-phenothiazinium (**PPT**$^{\bullet+}$) and 3-(pyrid-2-yl)-10-methyl-10*H*-phenothiazinium (**MPTP**$^{\bullet+}$). EPR spectra and corresponding calculations indicate phenothiazinium radical cations with minimal spin on the pyridine nitrogen. Addition of hindered phenols causes the radical cations to decay, and protonated products and the corresponding phenoxyl radicals to form. The ΔG° values for the formation of intermediates (determined through cyclic voltammetry and pK_a measurements) rule out a stepwise mechanism, and kinetic isotope effects support concerted proton–electron transfer (CPET) as the mechanism. Calculations indicate that the reaction of **PPT**$^{\bullet+}$ + ^{t}Bu$_3$PhOH undergoes a significant conformational change with steric interactions on the diabatic surface while maintaining the hydrogen bond; in contrast, **MPTP**$^{\bullet+}$ + ^{t}Bu$_3$PhOH maintains its conformation throughout the reaction. This difference is reflected in both experiment and calculations with $\Delta G^{\ddagger}_{\mathbf{MPTP}^{\bullet+}} < \Delta G^{\ddagger}_{\mathbf{PPT}^{\bullet+}}$ despite $\Delta G^{\circ}_{\mathbf{MPTP}^{\bullet+}} > \Delta G^{\circ}_{\mathbf{PPT}^{\bullet+}}$. Experimental results with 2,6-di-*tert*-butyl-4-methoxyphenol are similar. Hence, despite the structural similarity between the compounds, differences in the inner sphere component for CPET affect the kinetics.

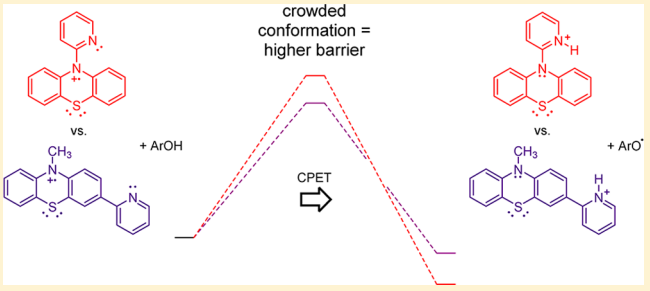

INTRODUCTION

Radical chemistry is a dominant paradigm in organic chemistry, and hydrogen atom transfer (HAT) is an important mechanism in this paradigm. In HAT, the H$^+$ and e$^-$ transfer from the same bond. HAT has been contrasted to concerted proton–electron transfer (CPET) for which the H$^+$ is transferred between lone pairs in a hydrogen bond and the e$^-$ is transferred between different orbital systems.[1] Some examples include reactions with phenols,[2] oximes,[3] flavins,[4] tryptophan,[5] guanosine,[6] and structurally related compounds. CPET also extends to cases not usually considered as HAT, such as reactions for which the H$^+$ and e$^-$ are transferred to or from multiple reagents, sites, or orbitals, and is sometimes qualified with "bidirectional".[7] (However, the orbital distinction between CPET and HAT can be ambiguous,[8] and it has been suggested that the degree of nonadiabaticity is a better criterion.[9])

Tethering a one-electron oxidant and a base generates a reagent that is capable of undergoing CPET. Several groups are using these systems to investigate what structures allow for CPET and how the structure affects the rate and thermodynamics for the reactions. For example, insertion of a spacer between the oxidant and base[10] or increasing the distance of H$^+$ transfer[11] slows the overall kinetics. Here we describe two radical cations with appended bases (**PPT**$^{\bullet+}$ and **MPTP**$^{\bullet+}$, Figure 1) and investigate their reactivity with hindered phenols. (Hindered phenols were employed since the corresponding phenoxyl radicals are persistent and do not appear to couple with the radical cations or each other. They are common reaction partners in studies of CPET, in part because they are hydrogen bond donors and because they have high-energy intermediates for the potential stepwise mechanisms.[8b]) As described below, **PPT**$^{\bullet+}$ undergoes a significant conformational shift during its reaction with hydrogen atom donors; this conformational shift results in a larger barrier for reaction compared with **MPTP**$^{\bullet+}$, which does not undergo as dramatic a shift. This is interpreted as a difference in the inner sphere reorganization, in parallel to electron transfer.

Received: June 23, 2015
Published: August 13, 2015

DOI: 10.1021/acs.joc.5b01427
J. Org. Chem. 2015, 80, 8705–8712

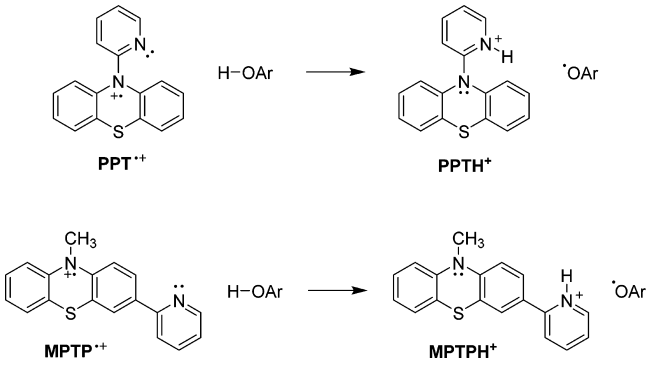

Figure 1. Reactions with 10-(2-pyridyl)-10*H*-phenothiazinium (**PPT**$^{\bullet+}$) and 3-(pyrid-2-yl)-10-methyl-10*H*-phenothiazinium (**MPTP**$^{\bullet+}$).

RESULTS

The radical cations were synthesized by palladium-catalyzed couplings and one-electron oxidation. Radical cation precursor 10-(pyridin-2-yl)-10*H*-phenothiazine (**PPT**)[12] was synthesized by a Buchwald–Hartwig amination,[13] and 3-(pyrid-2-yl)-10-methyl-10*H*-phenothiazine (**MPTP**) was synthesized from the known pinacol borane[14] via a Suzuki coupling.[15] Cyclic voltammetry (CV) of the neutral compounds provided a reversible wave at 0.39 ± 0.03 and 0.32 ± 0.03 V, for **PPT**$^{\bullet+/0}$ and **MPTP**$^{\bullet+/0}$, respectively, vs $Cp_2Fe^{+/0}$ in 0.1 M NBu_4PF_6 in MeCN (Figures S6 and S7). Similar systems undergo reversible CV.[16] Forming the radical cations in solution requires an oxidant with a reduction potential higher than that of the radical cation–neutral pair. Lewis acidic oxidants such as metal ions and other strong electrophiles (e.g., NO^+) reacted with the pyridine lone pair. Oxidations with limiting tris(4-bromophenyl)aminium hexafluorophosphate (E = 0.67 V vs $Cp_2Fe^{+/0}$;[17] E_{rxn} = 0.28 V ≡ K_{eq} = 5.2 × 10^4 for $NAr^{Br}_3{}^{\bullet+}$ + **PPT** ⇌ NAr^{Br}_3 + **PPT**$^{\bullet+}$; and E_{rxn} = 0.35 V ≡ K_{eq} = 1.2× 10^8 for $NAr^{Br}_3{}^{\bullet+}$ + **MPTP** ⇌ NAr^{Br}_3 + **MPTP**$^{\bullet+}$) provide colored solutions, red for **PPT**$^{\bullet+}$ and purple for **MPTP**$^{\bullet+}$. Absorptions at 515 (ε = 1.0 × 10^4), 779 (1.5 × 10^3), and 890 nm (1.4 × 10^3 M^{-1} cm^{-1}) for **PPT**$^{\bullet+}$ (Figure S2) and 580 (9.8 × 10^3), 779 (2.0 × 10^3), and 864 nm (1.9 × 10^3 M^{-1} cm^{-1}) in MeCN for **MPTP**$^{\bullet+}$ (Figure S5) in the UV–vis spectrum are indicative of phenothiazinium radical cations.[18] Solutions of **PPT**$^{\bullet+}$ at ≤10 mM maintain their absorbance in the UV–vis over several days in air (loss of absorbance per day ~2–3%). EPR spectra were recorded in CH_2Cl_2 (Figure S9 and Tables S1 and S2), and ^{1}H NMR spectra in CD_3CN are silent. The persistence of the radical cation echoes that of substituted phenothiazinium[19] and related aminium radical cations[20] in the presence of pyridine.

Hindered phenols were employed as hydrogen atom donors (Figure 1). Addition of excess 2,4,6-tri-*tert*-butylphenol (^{t}Bu$_3$PhOH, 1–10 mM) to the radical cations (0.1–0.3 mM) in CH_3CN causes a decay in the absorptions and appearance of peaks for ^{t}Bu$_3$PhO$^\bullet$ at 400 and 626 nm.[21] For **PPT**$^{\bullet+}$, the resulting solutions were colorless with no significant absorptions for **PPTH**$^+$; the concentration of ^{t}Bu$_3$PhO$^\bullet$ was small enough to not provide visible color. For **MPTP**$^{\bullet+}$, resulting solutions are intensely yellow corresponding to **MPTPH**$^+$ (λ_{max} = 415 nm, ε = 9.6 × 10^3 M^{-1} cm^{-1}), confirmed by the protonation of **MPTP** with dimethylformamide–triflic acid complex. The decay was monitored by stopped flow under pseudo-first-order conditions. Rate constants were determined through global fitting. Plots of k_{obs} vs the concentration of phenol in excess provided second-order rate constants: 12 ± 1 and 790 ± 80 M^{-1} s^{-1} for **PPT**$^{\bullet+}$ and **MPTP**$^{\bullet+}$, respectively. Similar kinetics with ^{t}Bu$_3$PhOD provide kinetic isotope effects: $k_{D,PPT^{\bullet+}}$ = 4.7 ± 0.5 M^{-1} s^{-1} ≡ k_H/k_D = 2.6 ± 0.4; $k_{D,MPTP^{\bullet+}}$ = 90 ± 9 M^{-1} s^{-1} ≡ k_H/k_D = 8.7 ± 1.2. Activation parameters were determined for **PPT**$^{\bullet+}$ + ^{t}Bu$_3$PhOH over a range of 13.4–62.6 °C: $\Delta H^‡$ = 7.5 ± 0.3 kcal mol^{-1} and $\Delta S^‡$ = −28.4 ± 0.9 cal K^{-1} mol^{-1}. Similar kinetics using 2,6-di-*tert*-butyl-4-methoxyphenol (^{t}Bu$_2$(OMe)PhOH) as the hydrogen donor afford rate constants of (7.5 ± 0.7) × 10^3 and (9.0 ± 0.9) × 10^4 M^{-1} s^{-1} for **PPT**$^{\bullet+}$ and **MPTP**$^{\bullet+}$, respectively.

Additional experiments provide thermodynamic parameters. An acid–base equilibration study with thymol blue (pK_a = 13.4)[22] and **PPT** provided pK_a[**PPT**{**H**$^+$/^{0}}] = 10.9 ± 0.2. Addition of triflic acid to **PPT** in electrolyte solution caused a shift in the CV attributed to **PPTH**$^{2+/+}$ at 0.67 V. (CVs of protonated 10-ammoniumalkyl-10*H*-phenothiazines are reversible, even in water.[23]) An equilibration study with tris(4-tolyl)aminium (E = 0.38 V)[17] provides an equilibrium constant of 0.63, consistent with E[**PPT**$^{\bullet+/0}$] = 0.39 V. These data provide an effective bond dissociation free energy (BDFE) for **PPTH**$^+$ → **PPT**$^{\bullet+}$ + H$^\bullet$ of 79 ± 1 kcal/mol. The pK_a of **MPTP**{**H**$^{+/0}$} was determined by titration with pyridinium (pK_a = 12.6)[23] and monitoring the growth of **MPTPH**$^+$ to provide pK_a = 11.9. Further parallel experiments provided E[**MPTPH**$^{2+/+}$] = 0.51 V and the effective BDFE for **MPTPH**$^+$ → **MPTP**$^{\bullet+}$ + H$^\bullet$ of 79 ± 1 kcal/mol. The kinetic and thermodynamic data are summarized in Table 1.

Table 1. Experimental and Calculated Parameters for Radical Cations

	PPT$^{\bullet+}$	**MPTP**$^{\bullet+}$
pK_a (XPTH$^+$ → XPT + H$^+$)	10.9 ± 0.1	11.9 ± 0.1
E (XPT$^{\bullet+/0}$, V)	0.39 ± 0.03	0.32 ± 0.01
BDFE (kcal/mol)	78.8 ± 0.8	78.6 ± 0.8
E (XPTH$^{2+/+}$, V)	0.67 ± 0.03	0.51 ± 0.03
$k_{2,4,6\text{-}^t\text{Bu}_3\text{PhOH}}$ (M^{-1} s^{-1})	12 ± 1	790 ± 80
$k_{2,4,6\text{-}^t\text{Bu}_3\text{PhOD}}$ (M^{-1} s^{-1})	4.7 ± 0.5	90 ± 9
k_H/k_D	2.6 ± 0.4	8.7 ± 1.2
$k_{2,6\text{-}^t\text{Bu}_2\text{(MeO)PhOH}}$ (M^{-1} s^{-1})	7.5 × 10^3	9 × 10^4

Since **PPT**$^{\bullet+}$, **MPTP**$^{\bullet+}$, and **MPTPH**$^+$ have significant absorptions in the visible region, several equilibration experiments were performed between the sets of compounds to determine proton, electron, and proton–electron equilibrium constants (Table 2). For example, an equilibration experiment provides an alternate method to find the BDFE for **MPTPH**$^+$. The equilibrium constant for ^{t}Bu$_3$PhOH + **MPTP**$^{\bullet+}$ ⇌ ^{t}Bu$_3$PhO$^\bullet$ + **MPTPH**$^+$ of 9.8 ± 0.9 provides $\Delta G°$ = −1.1 ± 0.1 kcal/mol, and the literature BDFE for ^{t}Bu$_3$PhOH of 77.1 kcal/mol[8b] provides a consistent BDFE of 78.8 ± 1.3 kcal/mol.

Table 2. Experimentally Determined Equilibrium Constants and $\Delta G°$

equilibrium	K_{eq}	$\Delta G°$ (kcal/mol)
PPT + **MPTPH**$^+$ ⇌ **PPTH**$^+$ + **MPTP**	0.17	−1.1 ± 0.1
PPT + **MPTP**$^{\bullet+}$ ⇌ **PPT**$^{\bullet+}$ + **MPTP**	0.031	−2.1 ± 0.1
PPTH$^+$ + **MPTP**$^{\bullet+}$ ⇌ **PPT**$^{\bullet+}$ + **MPTPH**$^+$	0.32	−0.7 ± 0.1
MPTP$^{\bullet+}$ + ^{t}Bu$_3$PhOH ⇌ **MPTPH**$^+$ + ^{t}Bu$_3$PhO$^\bullet$	9.8	1.4 ± 0.1

DOI: 10.1021/acs.joc.5b01427
J. Org. Chem. 2015, 80, 8705–8712

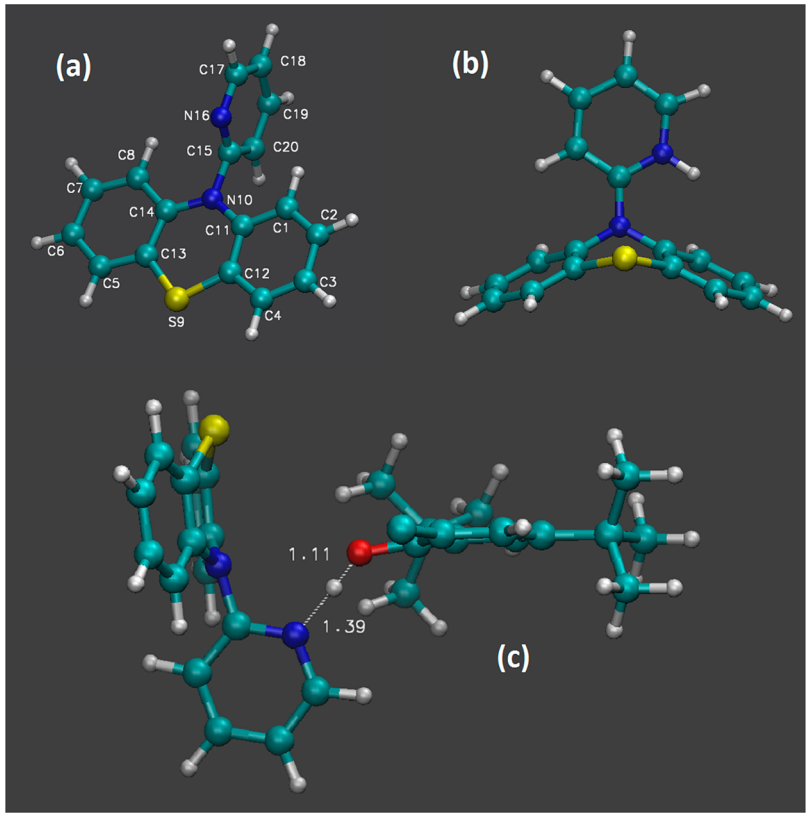

Figure 2. (a) **PPT**$^{\bullet+}$ with numbering, (b) **PPTH**$^{+}$, and (c) calculated TS for **PPT**$^{\bullet+}$ + ^{t}Bu$_3$PhOH → **PPTH**$^{+}$ + ^{t}Bu$_3$PhO$^{\bullet}$. One *tert*-butyl group has been truncated to a single carbon to aid in visualizing the TS geometry.

(Reactions with **PPT**$^{\bullet+}$ were slow to come to equilibrium at the appropriate concentrations to measure the corresponding equilibrium constant.)

Calculations were performed on the radical cations, the protonated products, ^{t}Bu$_3$PhOH, and both pre- and post-reaction hydrogen bonded complexes (i.e., ^{t}Bu$_3$PhOH···**PPT**$^{\bullet+}$, ^{t}Bu$_3$PhO$^{\bullet}$···**PPTH**$^{+}$, ^{t}Bu$_3$PhOH···**MPTP**$^{\bullet+}$, and ^{t}Bu$_3$PhO$^{\bullet}$···**MPTPH**$^{+}$). In addition, the classical transition states (TS) were located. All calculations were performed in Gaussian 09[24] using the B972 model chemistry[25] and the 6-31+G(d,p) basis set.[26]

The pyridine ring of **PPT**$^{\bullet+}$ is orthogonal to the planar phenothiazine ring (Figure 2) as in other 10-aryl-10*H*-phenothiazinium radical cations.[27] The conformations of 9-phenylanthracene and related compounds are similar.[28] The singly occupied molecular orbital (SOMO) contains significant electron density on the phenothiazine ring but negligible density on the pyridine ring. (A more complete analysis of the molecular orbitals and spin densities appears in the Supporting Information.) The EPR spectrum has a small hyperfine coupling for the pyridyl N (2.75−3.00 MHz), indicating a 0.5−0.6% spin population on it; DFT calculations are consistent with this value. Figure S28 displays the spin density of **PPT**$^{\bullet+}$, contoured at an isovalue of 0.0025 au; the spin density is completely confined to the phenothiazine ring at this level. Qualitatively, the planar conformation allows the charge and spin density to be delocalized over the phenothiazine ring with minimal steric interaction with the hydrogens at positions 1 and 8. In **PPTH**$^{+}$, the phenothiazine N has pyramidalized. The phenothiazine is boat-like with the pyridine pseudoaxial, and the pyridine no longer bisects the phenothiazine ring. This conformation parallels many neutral 10-aryl-10*H*-phenothiazines.[29] The progression of the backbone conformational change during the CPET reaction is illustrated in Figures S30 and S31.

The TS geometry is intermediate between **PPT** and **PPTH**$^{+}$. The phenothiazine ring at the TS resembles the boat-like phenothiazine geometry of **PPTH**$^{+}$. However, the pyridine ring remains orthogonal as in **PPT**$^{\bullet+}$, but pseudoequatorial instead of pseudoaxial. This conformation is required to maintain the hydrogen bond while minimizing steric clashing with ^{t}Bu$_3$PhO$^{\bullet}$; the smallest *tert*-butyl hydrogen−sulfur distance is 3.42 Å, only slightly larger than what is expected from van der Waals radii. Vibrational frequency evaluation of the TS produced a single imaginary frequency (882.5 cm^{-1}). No stationary point was found for placing the pyridine in the pseudoaxial position. Starting from isolated ^{t}Bu$_3$PhOH and **PPT**$^{\bullet+}$, the calculated *in vacuo* $\Delta G^{\ddagger}$ is 14.7 kcal/mol, including a basis set superposition error of 1.8 kcal/mol. Static solvation of the *in vacuo* isolated reactant and TS geometries with the SMD[30] implicit solvation model resulted in a calculated $\Delta G^{\ddagger}$ of 21.8 kcal/mol. Calculations also were performed on the stable intermediates for both electron transfer (ET) and proton transfer (PT). Solvating the *in vacuo* optimized geometries of each reactant and stable intermediate with the SMD implicit solvation model provides ΔG_{PT} = 34.8 kcal/mol (190.7 kcal/mol *in vacuo*) and ΔG_{ET} = 10.5 kcal/mol (14.5 kcal/mol *in vacuo*). The value for *in vacuo* PT is extremely high due to charge-separation in the gas phase in contrast to ET or CPET.

The analogous reaction with **MPTP**$^{\bullet+}$ proceeds with a much less significant conformational change (Figure 3). The phenothiazine ring of **MPTP**$^{\bullet+}$ is nearly planar, and the

DOI: 10.1021/acs.joc.5b01427
J. Org. Chem. 2015, 80, 8705−8712

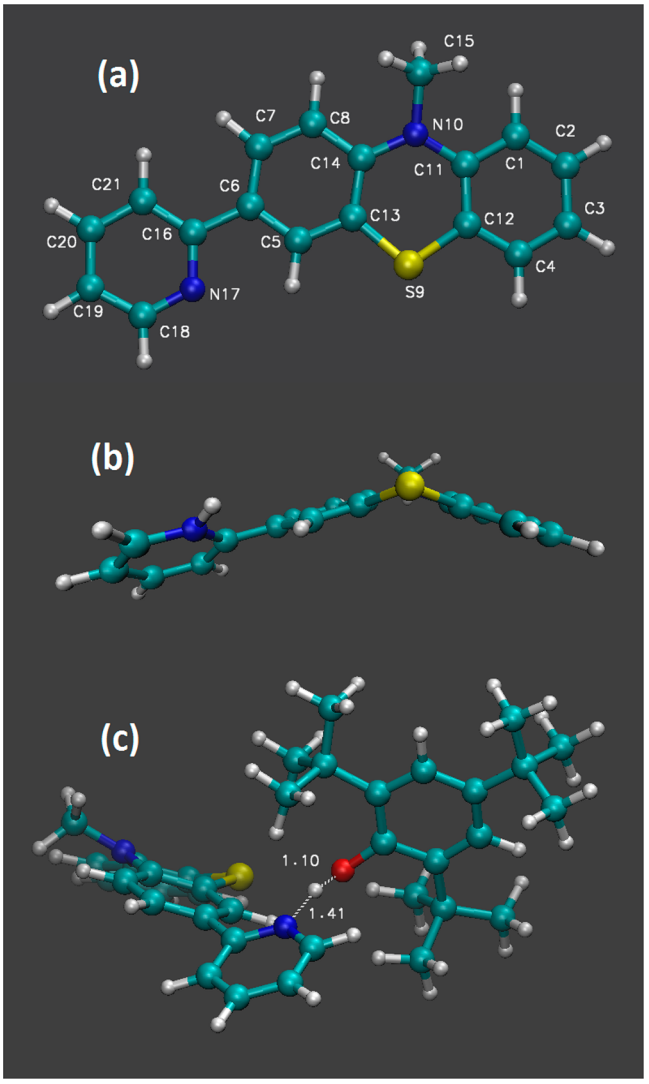

Figure 3. (a) **MPTP**$^{\bullet+}$ with numbering, (b) **MPTPH**$^{+}$, and (c) calculated TS for **MPTP**$^{\bullet+}$ + ^{t}Bu$_3$PhOH → **MPTPH**$^{+}$ + ^{t}Bu$_3$PhO$^{\bullet}$.

pyridine and phenothiazine rings are nearly coplanar in the radical cation, in contrast to the orthogonal positioning in **PPT**$^{\bullet+}$. Optimizations started with the pyridine orthogonal to the phenothiazine system resulted in the described pseudoplanar geometry. Experimentally, the hyperfine coupling to the phenothiazine nitrogen and the attached methyl group dominate the EPR spectrum, although a small amount of spin density is present on the attached, coplanar pyridine in the calculation (Figure S29). As for **PPTH**$^{+}$, the phenothiazine ring of **MPTPH**$^{+}$ is boat-like, but the methyl group is in the pseudoequatorial position. The pyridine ring in **MPTPH**$^{+}$ is tilted relative to the attached phenothiazine, occupying a position neither coplanar nor orthogonal to the phenothiazine ring.

In the TS, the geometry of the acceptor component remains similar to **MPTPH**$^{+}$. The phenothiazine ring is boat-like at the TS, the phenothiazine methyl is pseudoequatorial, and the pyridine is tilted out of the plane of the phenothiazine with a $N_{17}-C_{16}-C_6-C_5$ torsion angle of 39.4°. The transferring hydrogen remains closer to the O with O···H and N···H distances of 1.10 and 1.41 Å, respectively. These distances are similar to those at the TS for ^{t}Bu$_3$PhOH + **PPT**$^{\bullet+}$. Vibrational frequency evaluation of the ^{t}Bu$_3$PhOH···**MPTP**$^{\bullet+}$ TS produced a single imaginary frequency (709.3 cm^{-1}). Starting from isolated ^{t}Bu$_3$PhOH and **MPTP**$^{\bullet+}$, the calculated *in vacuo* $\Delta G^{\ddagger}$ is 10.1 kcal/mol (basis set superposition error 1.5 kcal/mol) and the solvated $\Delta G^{\ddagger}$ is 21.8 kcal/mol; calculations on the stable intermediates, including solvation, for both ET and PT provide ΔG_{PT} = 27.0 kcal/mol (170.6 kcal/mol *in vacuo*) and ΔG_{ET} = 12.9 kcal/mol (16.9 kcal/mol *in vacuo*).

DISCUSSION

In this work, two persistent and structurally similar base-appended radical cations are reacted with hindered phenols as hydrogen atom donors to explore the mechanism and compare the two compounds. Each compound combines a phenothiazinium radical cation and a pyridine, and hence each has the components to accept an e^{-} and a H^{+}. We will consider the mechanism for the two sets of reactions and then compare the two cases.

From experimental and literature data,[8b,31] ΔG° for ET and PT intermediates can be estimated and the $\Delta G^{\ddagger}$ can be calculated (from the Eyring equation) to explore the mechanism (see Table 3 and Experimental Section) . The

Table 3. Experimental and Computational Free Energies (kcal/mol)

	experimental			computational		
reactant pair	$\Delta G^{\ddagger}$	ΔG°_{ET}	ΔG°_{PT} (est.)	$\Delta G^{\ddagger}$	ΔG°_{ET}	ΔG°_{PT}[a]
PPT$^{\bullet+}$ + ^{t}Bu$_3$PhOH	15.9	18.2	29.9	14.7	14.5	34.8
PPT$^{\bullet+}$ + ^{t}Bu$_2$(OMe)PhOH	12.1	14.3	32.6			
MPTP$^{\bullet+}$ + ^{t}Bu$_3$PhOH	13.4	19.8	26.4	10.1	16.9	27.0
MPTP$^{\bullet+}$ + ^{t}Bu$_2$(OMe)PhOH	10.7	15.9	29.2			

[a]Calculated including implicit solvation.

data indicate ΔG_{ET} for **PPT**$^{\bullet+}$ + ^{t}Bu$_3$PhOH → **PPT** + ^{t}Bu$_3$PhOH$^{\bullet+}$ of 18.2 ± 1.4 kcal/mol and an estimated ΔG_{PT} for **PPT**$^{\bullet+}$ + ^{t}Bu$_3$PhOH → **PPTH**$^{2+}$ + Bu$_3$PhO^{-} of 29.9 kcal/mol. These ΔG° values are larger than the measured $\Delta G^{\ddagger}$ of 15.9 ± 0.7 kcal/mol. The corresponding data for ^{t}Bu$_2$(OMe)PhOH + **PPT**$^{\bullet+}$ are similar: ΔG_{ET} = 14.3 ± 1.4 kcal/mol; $\Delta G_{PT} \approx$ 32.6 kcal/mol; $\Delta G^{\ddagger}$ = 12.1 ± 0.7 kcal/mol. **MPTP**$^{\bullet+}$ has a similar pattern for the corresponding values: For reaction with ^{t}Bu$_3$PhOH, $\Delta G^{\ddagger}$ = 13.4 ± 0.7 kcal/mol, ΔG_{ET} = 19.8 ± 1.4 kcal/mol, and $\Delta G_{PT} \approx$ 26.4 kcal/mol, and with ^{t}Bu$_2$(OMe)-PhOH, $\Delta G^{\ddagger}$ = 10.7 ± 0.7 kcal/mol, ΔG_{ET} = 15.9 ± 1.4 kcal/mol, and $\Delta G_{PT} \approx$ 29.2 kcal/mol; these data are summarized in Table 3. These data suggest that CPET is the mechanism. (While ΔG_{ET} is close to being within error of the experiment, ET is unlikely to be barrierless.) Experimentally, $\Delta G^{\ddagger} < \Delta G^{\circ}_{ET} \ll \Delta G^{\circ}_{PT}$; the computed *in vacuo* values for ΔG°_{ET} and $\Delta G^{\ddagger}$, and the computed solvated value of ΔG°_{PT} are in reasonable agreement. The computed *in vacuo* difference between the barriers ($\Delta\Delta G^{\ddagger}$) of 4.6 kcal/mol echoes the experimental results (2.5 kcal/mol), with **MPTP**$^{\bullet+}$ reacting with a smaller barrier; including the effects of solvation in the calculations results in the barriers for both reactions being equal.

The kinetic isotope effects for the reactions with ^{t}Bu$_3$PhOH of 2.6 ± 0.4 and 8.9 ± 1.2 for **PPT**$^{\bullet+}$ and **MPTP**$^{\bullet+}$, respectively, indicate that the proton is involved in the rate-determining step. The latter value is likely out of the classical range[32]

DOI: 10.1021/acs.joc.5b01427
J. Org. Chem. 2015, 80, 8705−8712

suggesting a tunneling event, although measured kinetic isotope effects vary from small (~2)[33] to very large (>400)[34] for CPET reactions.[35] The difference between the two systems could be ascribed to a balance among several factors (e.g., hydrogen vibrational wave function overlap, frequency, reorganization energy, and ΔG°)[1a,36] and cannot be separated with the reported experimental and computational data.

Despite reactions with the **MPTP**$^{\bullet+}$ occurring with lower barriers than those with **PPT**$^{\bullet+}$, the **MPTP**$^{\bullet+}$ reactions are less favored thermodynamically. The ΔG° for the reaction can be determined in two ways from the thermodynamic data. (1) Using the $E[\mathrm{XPT}^{\bullet+/0}]$ and $pK_a[\mathrm{XPT}\{\mathrm{H}^{+/0}\}]$ values, one obtains BDFEs of 79.1 ± 0.8 and 78.6 ± 0.8 kcal/mol, respectively, for **PPTH**$^+$ → **PPT**$^{\bullet+}$ + H$^\bullet$ and **MPTPH**$^+$ → **MPTP**$^{\bullet+}$ + H$^\bullet$, implying that the reactions with the phenols are 0.5 ± 1.6 kcal/mol ($\Delta\Delta G^\circ$) further downhill for **PPT**$^{\bullet+}$ compared with **MPTP**$^{\bullet+}$. (2) A direct and more precise comparison can be determined from the equilibrium constant for **PPTH**$^+$ + **MPTP**$^{\bullet+}$ ⇌ **PPT**$^{\bullet+}$ + **MPTPH**$^+$; K_{eq} = 0.32 implies $\Delta\Delta G^\circ$ = 0.7 ± 0.1 kcal/mol. (This is also consistent with the value determined from combining the ET and PT equilibria, providing $\Delta\Delta G^\circ$ = 1.0 ± 0.3 kcal/mol.) The difference in the activation energies for reaction $\Delta\Delta G^\ddagger$ follow the reverse trend, − 2.5 ± 1.4 kcal/mol for reaction with ^{t}Bu$_3$PhOH and −1.4 ± 1.4 kcal/mol for reaction with ^{t}Bu$_2$(OMe)PhOH. For most CPET reactions with reagents of similar structure, the driving force and activation energy are correlated for similar reactions, with a lower activation energy for a more exergonic reaction such as in a Marcus relationship.[37] Hence, although both **PPT**$^{\bullet+}$ and **MPTP**$^{\bullet+}$ have a pyridine appended to a phenothiazinium radical cation, the order of activation energies is reversed.

The contrast between the geometry changes for the two systems explains the mismatch between the driving force of reaction and kinetics. As in other 10-aryl-10*H*-phenothiazine radical cations,[27] the calculations suggest that the pyridine ring of **PPT**$^{\bullet+}$ is orthogonal to the phenothiazine ring. This conformation allows for maximum overlap in the phenothiazine π system including the N p-type orbital.[27] The molecule resembles 10-phenylanthracene, which has a similar orthogonal conformation and a large barrier (>20 kcal/mol) to rotation with a distorted TS.[28] The nitrogen pyramidalizes upon accepting the e$^-$ as in neutral, closed-shell phenothiazines.[29] This is reflected in the TS with a partially pyramidalized N. The hydrogen bond between ^{t}Bu$_3$PhOH and **PPT**$^{\bullet+}$ must be maintained for the H$^+$ to be transferred, and hence placing the pyridine in the pseudoaxial position would produce severe steric interactions for the phenothiazine ring and the *tert*-butyl groups. The pyridine is thus forced into the crowded pseudoequatorial position in the TS. In contrast, the geometry of **MPTP**$^{\bullet+}$ closely resembles that of **MPTPH**$^+$ with fewer constraints at the TS. That the **MPTP**$^{\bullet+}$ reactions are inherently faster than the **PPT**$^{\bullet+}$ reactions despite a lower driving force suggests that the inner sphere reorganization reflected in the conformational changes are the best explanation for the differences in these compounds, paralleling similar effects in electron transfer reactivity.[38] (However, the calculations reflect a diabatic surface, while the CPET reaction is likely to be nonadiabatic.)

Recently, distances between electron donating and accepting sites have been related to kinetics, with an increased distance slowing the reaction.[10] In the CPET reactions presented here, the distances between electron donating and accepting sites and between proton donating and accepting sites are not significantly different. The electron transfer distance is difficult to compare; however, the pyridine ring acts as a discrete spacer between the phenothiazine and the phenols for both the **PPT**$^{\bullet+}$ and **MPTP**$^{\bullet+}$ radical cations. Furthermore, the frontier orbitals are similar in terms of contributions between the two components.

In conclusion, a persistent pyridyl-appended radical cation abstracts a net hydrogen atom from a phenol by CPET, with separate sites for accepting the H$^+$ and e$^-$. The systems have different conformation changes: reaction with **PPT**$^{\bullet+}$ requires a more constrained TS than for **MPTP**$^{\bullet+}$, and this difference in inner-sphere reorganization increases the TS energy.

EXPERIMENTAL SECTION

General Considerations. Acetonitrile for kinetics and equilibration studies was purchased dry and used under N_2. Toluene was either distilled from Na/benzophenone under N_2 or taken from a solvent drying column before use. Methylene chloride was taken from a solvent drying system. Triethylamine was distilled from sodium hydroxide under nitrogen, and 1,4-dioxane was also refluxed and dried over benzophenone and Na under nitrogen. The cyclic voltammogram for 1,3-di-*tert*-butyl-2,5-dimethoxybenzene was taken under nitrogen in a glovebox.

Room-temperature electron paramagnetic resonance (EPR) measurements were taken using 140 μL of solution in a 4 mm o.d. quartz tube. Samples were prepared and filled into quartz tubes in the glovebox and capped with a rubber septum and parafilm, and the EPR spectrum was measured immediately after. Complete analysis of the EPR spectra is given in the Supporting Information.

Synthesis. 2,4,6-Tri-*tert*-butylphenol-O-*d* was synthesized by the procedure of Stack and co-workers.[39] 1,3-Di-*tert*-butyl-2,5-dimethoxybenzene was synthesized by deprotonating the phenol with NaH in DMF and alkylating with methyl iodide.[40] Tri-(*p*-tolyl)aminium hexafluorophosphate and tri-(*p*-bromophenyl)aminium hexafluorophosphate were synthesized using the neutral amine and $AgPF_6$ and I_2[41] or with $NOPF_6$.[42] 10-Methyl-3-(4,4,5,5-tetramethyl-1,3,2-dioxaborolan-2-yl)-10*H*-phenothiazine was synthesized by the procedure of Müller and co-workers.[14]

Synthesis of 10-(Pyridin-2-yl)-10H-phenothiazine.[43−46] To 25 mL of dry toluene was added phenothiazine (1.794 g, 9.00 mmol), sodium *tert*-butoxide (1.394 g), DPPF (1,1′-bis(diphenylphosphino)ferrocene, 32.2 mg), 2-bromopyridine (0.996 mL, 1.643 g, 10.4 mmol), and $Pd_2(dba)_3$ (40.2 mg; dba = dibenzylideneacetone), in that order. The reaction was refluxed overnight. Additional $Pd_2(dba)_3$ (38 mg) and DPPF (30 mg) were added after 24 h, and the mixture was refluxed overnight. The reaction was filtered through silica, which was washed with ethyl acetate, and the solvent was removed under reduced pressure. The compound was subjected to column chromatography (20/1 to 12/1 v/v hexanes/ethyl acetate gradient) to afford a solid (1.829 g, 73.5%). ^{1}H NMR (300 MHz, $CDCl_3$, Figure S1): δ 8.28 (dd, J = 8.0, 2.0 Hz, 1H), 7.56 (d, J = 13.3 Hz, 2H), 7.52−7.44 (m, 1H), 7.38 (dd, J = 12.8, 2.0 Hz, 2H), 7.32−7.24 (m, 2H), 7.18−7.11 (m, 2H), 6.93 (d, J = 14.1 Hz, 1H), 6.87 (dd, J = 11.7, 8.5 Hz, 1H). Mp 109.6−110.4 °C.[45] The compound was recrystallized twice to a colorless solid from 1/1 v/v hexanes/ethyl acetate before use in kinetics and equilibration studies.

Synthesis of 10-Methyl-3-(pyridin-2-yl)-10H-phenothiazine.[15] A combination of 10-methyl-3-(4,4,5,5-tetramethyl-1,3,2-dioxaborolan-2-yl)-10*H*-phenothiazine (5.6 g, 1.64 mmol), $Pd_2(dba)_3$ (0.0329 g, 0.0573 mmol), and DPPF (0.0295 g, 0.0532 mmol) was added to a 2.0 M aqueous solution of Na_2CO_3 (2.454 mL) and 2-propanol (12 mL), which was degassed by bubbling with nitrogen. This reaction was stirred and refluxed under nitrogen for 56 h at 70 °C, when the reaction was deemed complete by TLC. Water was added to this reaction mixture, and the organic layer was extracted with three portions of Et_2O. These organic layers were collected, combined, and dried over $MgSO_4$. Column chromatography was used to purify the

DOI: 10.1021/acs.joc.5b01427
J. Org. Chem. 2015, 80, 8705−8712

compound (hexanes/ethyl acetate, 20:1 to 8:1), which results in isolated compound as a solid (0.376 g, 1.26 mmol, 46%). ^{1}H NMR (300 MHz, $CDCl_3$, Figure S3) δ 6.66 (m, 1H), 7.87 (m), 7.74 (m), 7.67(m), 7.19 (m), 6.96 (m), 6.89 (m), 3.44 (s, 3H) ppm. ^{13}C NMR (400 MHz, $CDCl_3$, Figure S4) δ 35.4, 114.09, 114.14, 119.6, 121.7, 122.7, 123.1, 123.8, 125.4, 126.0, 127.2, 127.5, 133.7, 136.7, 145.4, 146.5, 149.6, 156.3 ppm. Anal. Calcd for $C_{18}H_{14}N_2S$: C, 74.45; H, 4.86; N, 9.65. Found: C, 74.06; H, 4.84; N, 9.56.

In Situ Generation of Radical Cation. The radical cation was synthesized by combining a solution of tris(*p*-bromophenyl)aminium hexafluorophosphate and a solution of excess **PPT** in acetonitrile. Concentrations for kinetics were typically ~0.2 mM in **PPT** and ~0.1 mM for tris(*p*-bromophenyl)aminium hexafluorophosphate, although concentrations up to 1 mM were stable. The reaction was assumed to reach completion. Higher concentrations of **PPT** did not affect the kinetics. Solutions for EPR were made similarly in CH_2Cl_2.

Cyclic Voltammetry. Cyclic voltammetry was performed in 0.1 M Bu_4NPF_6 in acetonitrile with a glassy carbon working electrode, Ag/$AgNO_3$ (0.01 M) reference electrode, and platinum wire auxiliary electrode. Ferrocene was added as an internal standard. Cyclic voltammograms are provided in the SI (Figures S6–S8).

Thermodynamic Parameters for ^{t}Bu$_3$PhOH and ^{t}Bu$_2$(OMe)PhOH and Calculation of ΔG_{ET} and ΔG_{PT}. Thermodynamic parameters for ^{t}Bu$_3$PhOH are known: $E[^t\text{Bu}_3\text{PhOH}^{\bullet+/0}]$ = 1.18 V and $pK_a[^t\text{Bu}_3\text{PhO}\{\text{H}/^-\}]$ = 28.[8b,31] $E[^t\text{Bu}_2(\text{OMe})\text{PhOH}^{\bullet+/0}]$ can be estimated to be 1.01 V from a experimentally determined CV on neutral ^{t}Bu$_2$(OMe)PhOMe referencing to $Cp_2Fe^{+/0}$ (Figure S8). The pK_a for 2,6-di-*tert*-butyl-4-methoxyphenol was estimated by the method of Kütt el al.[47] using a value of 18.2 in DMSO:[8b,48] 0.980 × 18.2 + 12.31 = 30.1. The free energy difference for ET is determined by, for example, $\Delta G_{ET} = -nF(E[\mathbf{PPT}^{\bullet+/0}] - E[^t\text{Bu}_3\text{PhOH}^{\bullet+/0}])$. The free energy difference for PT is determined by a thermodynamic cycle as follows:

$$^t\text{Bu}_3\text{PhOH} \rightarrow {}^t\text{Bu}_3\text{PhO}^- + \text{H}^+ \qquad \Delta G^\circ = 2.303\ \text{RT}\ pK_{a1}$$

$$\mathbf{PPT} + \text{H}^+ \rightarrow \mathbf{PPTH}^+ \qquad \Delta G^\circ = -2.303\ \text{RT}\ pK_{a2}$$

$$\mathbf{PPT}^{\bullet+} + e^- \rightarrow \mathbf{PPT} \qquad \Delta G^\circ = -nFE_1$$

$$\underline{\mathbf{PPTH}^+ \rightarrow \mathbf{PPTH}^{2+} + e^-} \qquad \underline{\Delta G^\circ = nFE_2}$$

$$\mathbf{PPT}^{\bullet+} + {}^t\text{Bu}_3\text{PhOH} \rightarrow \mathbf{PPTH}^{2+} + {}^t\text{Bu}_3\text{PhO}^- \qquad \Delta G_{PT} = \Sigma\{\Delta G^\circ\}$$

Values of $\Delta G^\ddagger$ were determined using the rate constants and the Eyring equation ($\Delta G^\ddagger = -RT\ \ln[(kh)/(k_BT)]$) and are reported at 298 K.

Equilibration Studies. Graphs and UV–vis spectra are provided in the Supporting Information for these experiments. Reaction between $\mathbf{PPT}^{\bullet+}$ and ^{t}Bu$_3$PhOH was too slow to provide an accurate equilibrium constant. Errors are estimated at 10% for these experiments. Linear fits were to $y = mx + b$, but the y-intercepts were negligible in all cases.

Electron Transfer Equilibrium. The equilibrium constant for tris(4-tolyl)aminium and **PPT** was determined by adding 50 μL aliquots of a 12.1 mM solution of **PPT** to 3.0 mL of a 0.079 mM solution of tris(4-tolyl)aminium hexafluorophosphate solution. The absorbance at 668 nm, corresponding to an absorption of the aminium, was used to determine $[\text{NAr}^{\text{Me}}{}_3{}^{\bullet+}]$ (at equilibrium) after correcting for volume (Figure S10). The other concentrations were determined by mass balance. The slope of a plot of $[\mathbf{PPT}^{\bullet+}][\text{NAr}^{\text{Me}}{}_3]/[\text{NAr}^{\text{Me}}{}_3{}^{\bullet+}]$ vs [**PPT**] provided the equilibrium constant (Figure S11).

The equilibrium constant for **PPT** + $\mathbf{MPTP}^{\bullet+}$ ⇌ $\mathbf{PPT}^{\bullet+}$ + **MPTP** was determined by adding 50 μL aliquots of a 20.7 mM solution of **PPT** to 3.0 mL of a 83.7 μM solution of $\mathbf{MPTP}^{\bullet+}$. The absorbances at 515 and 580 nm, corresponding to λ_{max} of $\mathbf{PPT}^{\bullet+}$ and $\mathbf{MPTP}^{\bullet+}$, were used to determine their concentrations (by solving $abs_{515} = \varepsilon_{515,\text{PPT}^{\bullet+}}[\mathbf{PPT}^{\bullet+}] + \varepsilon_{515,\text{MPTP}^{\bullet+}}[\mathbf{MPTP}^{\bullet+}]$ and $abs_{580} = \varepsilon_{580,\text{PPT}^{\bullet+}}[\mathbf{PPT}^{\bullet+}] + \varepsilon_{580,\text{MPTP}^{\bullet+}}[\mathbf{MPTP}^{\bullet+}]$; Figure S16). The other concentrations were determined by mass balance. The slope of a plot of $[\mathbf{PPT}^{\bullet+}][\mathbf{MPTP}]/[\mathbf{MPTP}^{\bullet+}]$ vs [**PPT**] provided the equilibrium constant (Figure S17).

Proton Transfer Equilibrium. The equilibrium constant for **PPT** + $\mathbf{MPTPH}^+$ ⇌ $\mathbf{PPTH}^+$ + **MPTP** was determined by adding 50 μL aliquots of a 25.4 mM solution of **PPT** to 3.0 mL of an 83.3 μM solution of $\mathbf{MPTPH}^+$. The absorbance at 415 nm, corresponding to an absorption of the $\mathbf{MPTPH}^+$ (ε = 9.6 × 10^3 M^{-1} cm^{-1}), was used to determine $[\mathbf{MPTPH}^+]$ at equilibrium after correcting for volume (Figure S18). The other concentrations were determined by mass balance. The slope of a plot of $[\mathbf{PPTH}^+][\mathbf{MPTP}]/[\mathbf{PPTH}^+]$ vs [**PPT**] provided the equilibrium constant (Figure S19).

Proton–Electron Transfer Equilibrium. The equilibrium constant for $\mathbf{PPTH}^+$ + $\mathbf{MPTP}^{\bullet+}$ ⇌ $\mathbf{PPT}^{\bullet+}$ + $\mathbf{MPTPH}^+$ was determined by adding 50 μL aliquots of a 3.58 mM solution of $\mathbf{PPTH}^+$ to 3.0 mL of an 81.3 μM solution of $\mathbf{MPTP}^{\bullet+}$. Absorbances at 422, 515, and 580 nm were used to determine the concentrations of $\mathbf{MPTPH}^+$, $\mathbf{PPT}^{\bullet+}$, and $\mathbf{MPTP}^{\bullet+}$ (by solving $abs_{422} = \varepsilon_{422,\text{PPT}^{\bullet+}}[\mathbf{PPT}^{\bullet+}] + \varepsilon_{422,\text{PTP}^{\bullet+}}[\mathbf{MPTP}^{\bullet+}] + \varepsilon_{422,\text{PTPH}^+}[\mathbf{MPTPH}^+]$; $abs_{515} = \varepsilon_{515,\text{PPT}^{\bullet+}}[\mathbf{PPT}^{\bullet+}] + \varepsilon_{515,\text{PTP}^{\bullet+}}[\mathbf{MPTP}^{\bullet+}] + \varepsilon_{515,\text{PTPH}^+}[\mathbf{MPTPH}^+]$; and $abs_{580} = \varepsilon_{580,\text{PPT}^{\bullet+}}[\mathbf{PPT}^{\bullet+}] + \varepsilon_{580,\text{PTP}^{\bullet+}}[\mathbf{MPTP}^{\bullet+}] + \varepsilon_{580,\text{PTPH}^+}[\mathbf{MPTPH}^+]$; Figure S20). [**PPT**] was determined by mass balance. The slope of a plot of $[\mathbf{PPT}^{\bullet+}][\mathbf{MPTPH}^+]/[\mathbf{MPTP}^{\bullet+}]$ vs $[\mathbf{PPTH}^+]$ provided the equilibrium constant (Figure S21).

The equilibrium constant for $\mathbf{MPTP}^{\bullet+}$ + ^{t}Bu$_3$PhOH ⇌ $\mathbf{MPTPH}^+$ + ^{t}Bu$_3$PhO$^\bullet$ was determined by adding 50 μL aliquots of a 1.75 mM solution of ^{t}Bu$_3$PhOH to 3.0 mL of a 71.8 μM solution of $\mathbf{MPTP}^{\bullet+}$ under N_2. The absorbances at 422 and 580 nm were used to determine the concentrations of $\mathbf{MPTPH}^+$ and $\mathbf{MPTP}^{\bullet+}$ (by solving $abs_{422} = \varepsilon_{422,\text{PTP}^{\bullet+}}[\mathbf{MPTP}^{\bullet+}] + \varepsilon_{422,\text{PTPH}^+}[\mathbf{MPTPH}^+]$ and $abs_{580} = \varepsilon_{580,\text{PTP}^{\bullet+}}[\mathbf{MPTP}^{\bullet+}] + \varepsilon_{580,\text{PTPH}^+}[\mathbf{MPTPH}^+]$; Figure S22). Concentrations of ^{t}Bu$_3$PhOH and ^{t}Bu$_3$PhO were determined by mass balance. The slope of a plot of $[\mathbf{MPTPH}^+][^t\text{Bu}_3\text{PhO}^\bullet]/[\ \mathbf{MPTP}^{\bullet+}]$ vs $[^t\text{Bu}_3\text{PhOH}]$ provided the equilibrium constant (Figure S23).

Acid–Base Equilibrium for pK_a Determination. The equilibrium constant for **PPT** and thymol blue ($pK_a[\text{TH}_2 \rightleftharpoons \text{TH}^- + \text{H}^+, \text{MeCN}]$ = 13.4[22]) was determined by adding 50 μL aliquots of a 12.1 mM solution of **PPT** to 3.0 mL of a 0.89 mM solution of thymol blue solution. The absorbance at 395 nm (λ = 1.65 × 10^4 M^{-1} cm^{-1}), corresponding to an absorption of the deprotonated thymol blue (TH^-),[22] was used to determine $[TH^-]$ after correcting for volume, and the other concentrations were determined by mass balance (Figure S12). The slope of a plot of $[\mathbf{PPTH}^+][TH^-]/[TH_2]$ vs [**PPT**] provided the equilibrium constant (Figure S13).

Similarly, the equilibrium constant for **MPTP** and pyridinium was determined by adding 50 μL aliquots of 29.2 mM pyridinium hexafluorophosphate (pK_a = 12.6)[49] to 3.00 mL of 98.7 μM **MPTP**. The absorbance at 415 nm (ε = 9.6 × 10^3 M^{-1} cm^{-1}) was used to determine $\mathbf{MPTPH}^+$, and the other concentrations were determined by mass balance (Figure S14). The slope of a plot of $[\mathbf{MPTH}^+][\text{pyr}]/[\text{pyrH}^+]$ vs [**MPTP**] provided the equilibrium constant (Figure S15).

Kinetics Studies. Solutions of radical cation were generated as above in concentrations of 0.1–0.2 mM in acetonitrile in a glovebox, and hydrogen atom donors (2,4,6-tri-*tert*-butylphenol or 2,6-di-*tert*-butyl-4-methoxyphenol) were prepared at 5–100× these concentrations. Solutions were combined in a stopped flow spectrophotometer, and the absorbance over a 200 nm range centered at 515 nm was observed. The decay of the spectra was fit globally to a first-order decay using Spec-Fit. The slope of k_{obs} vs concentration of hydrogen atom donor provided the second-order rate constants. Sample plots of data are given in Figures S24–S26.

Eyring Analysis. Kinetics were performed at five temperatures between 13.4 and 62.6 °C as above. The activation parameters ($\Delta H^\ddagger$ and $\Delta S^\ddagger$) were determined from a plot of $\ln(k/T)$ vs $1/T$ (Figure S27).

Computational Procedures. All calculations were performed using the keyword int=ultrafine in Gaussian09. This produces a pruned grid of 99 radial shells with 590 points per shell for numerical integration. Frequency evaluations also included the keyword int=(Acc2e=11) to force tighter convergence (10^{-11}) of the two-electron integrals as part of solving the CPHF equations.

DOI: 10.1021/acs.joc.5b01427
J. Org. Chem. 2015, 80, 8705–8712

The BSSE at the transition state was calculated as the average of two counterpoise calculations using two fragments each. In the first calculation, the transferring hydrogen atom was assigned to $^{t}Bu_3PhOH$ (the two fragments were $^{t}Bu_3PhOH$ and the radical cation form of the acceptor), and in the second the transferring hydrogen was assigned to the hydrogen acceptor (the two fragments were $^{t}Bu_3PhO^{\bullet}$ and the cationic form of the acceptor).

■ ASSOCIATED CONTENT

Supporting Information

The Supporting Information is available free of charge on the ACS Publications website at DOI: 10.1021/acs.joc.5b01427.

Experimental and computational details (PDF)

■ AUTHOR INFORMATION

Corresponding Authors

*E-mail: JeffreyWolbach@eurofinsUS.com.
*E-mail: irhile@albright.edu.

Notes

The authors declare no competing financial interest.

■ ACKNOWLEDGMENTS

I.J.R. gratefully acknowledges support from the American Chemical Society-Petroleum Research Fund (49447-UR4) and James M. Mayer (via NIH Award GM050422) for supplies and services for a sabbatical during which a portion of this research was performed. J.P.W. gratefully acknowledges XSEDE Grant TG-CHE120047 for computing resources used in part for this research. J.P.W. and I.J.R. gratefully acknowledge support from the Albright Creative Research Experiences program and Albright College. S.S. gratefully acknowledges support from the University of Washington.

■ REFERENCES

(1) (a) Hammes-Schiffer, S. *J. Am. Chem. Soc.* **2015**, *137*, 8860−71. (b) Warren, J. J.; Mayer, J. M. *Biochemistry* **2015**, *54*, 1863−78. (c) Solis, B. H.; Hammes-Schiffer, S. *Inorg. Chem.* **2014**, *53*, 6427−43. (d) Migliore, A.; Polizzi, N. F.; Therien, M. J.; Beratan, D. N. *Chem. Rev.* **2014**, *114*, 3381−465. (e) Weinberg, D. R.; Gagliardi, C. J.; Hull, J. F.; Murphy, C. F.; Kent, C. A.; Westlake, B. C.; Paul, A.; Ess, D. H.; McCafferty, D. G.; Meyer, T. J. *Chem. Rev.* **2012**, *112*, 4016−93. (f) Saveant, J.-M. *Annu. Rev. Anal. Chem.* **2014**, *7*, 537−60. (g) Reece, S. Y.; Nocera, D. G. *Annu. Rev. Biochem.* **2009**, *78*, 673−99.

(2) (a) Mayer, J. M.; Hrovat, D. R.; Thomas, J. L.; Borden, W. T. *J. Am. Chem. Soc.* **2002**, *124*, 11142−7. (b) DiLabio, G. A.; Johnson, E. R. *J. Am. Chem. Soc.* **2007**, *129*, 6199−6203.

(3) DiLabio, G. A.; Ingold, K. U. J. *J. Am. Chem. Soc.* **2005**, *127*, 6693−6699.

(4) (a) Silverman, R. B.; Zelechonok, Y. *J. Org. Chem.* **1992**, *57*, 6373−4. (b) Sawyer, D. T.; Calderwood, T. S.; Johlman, C. L.; Wilkins, C. L. *J. Org. Chem.* **1985**, *50*, 1409−1412. (c) Knappe, W. R. *Z. Naturforsch., B: Anorg. Chem., Org. Chem.* **1977**, *32*, 434−437. (d) Huvaere, K.; Cardoso, D. R.; Homem-de-Mello, P.; Westermann, S.; Skibsted, L. H. *J. Phys. Chem. B* **2010**, *114*, 5583−5593. (e) Williams, R. F.; Bruice, T. C. *J. Am. Chem. Soc.* **1976**, *98*, 7752−7768.

(5) (a) Gagliardi, C. J.; Binstead, R. A.; Thorp, H. H.; Meyer, T. J. *J. Am. Chem. Soc.* **2011**, *133*, 19594−19597. (b) Zhang, M.; Hammarström, L. *J. Am. Chem. Soc.* **2011**, *133*, 8806−8809.

(6) Murakami, H.; Esaka, Y.; Nakayama, T.; Uno, B. *Chem. Lett.* **2011**, *40*, 268−269.

(7) (a) Biczók, L.; Gupta, N.; Linschitz, H. *J. Am. Chem. Soc.* **1997**, *119*, 12601−12609. (b) Biczók, L.; Linschitz, H. *J. Phys. Chem.* **1995**, *99*, 1843−1845.

(8) (a) Foti, M. C.; Daquino, D.; Mackie, I. D.; DiLabio, G. A.; Ingold, K. U. *J. Org. Chem.* **2008**, *73*, 9270−9282. (b) Warren, J. J.; Tronic, T. A.; Mayer, J. M. *Chem. Rev.* **2010**, *110*, 6961−7001.

(9) Hammes-Schiffer, S. *Energy Environ. Sci.* **2012**, *5*, 7696−7703.

(10) (a) Manner, V. W.; Mayer, J. M. *J. Am. Chem. Soc.* **2009**, *131*, 9874−9875. (b) Kuss-Petermann, M.; Wolf, H.; Stalke, D.; Wenger, O. S. *J. Am. Chem. Soc.* **2012**, *134*, 12844−12854. (c) Markle, T. F.; Tronic, T. A.; DiPasquale, A. G.; Kaminsky, W.; Mayer, J. M. *J. Phys. Chem. A* **2012**, *116*, 12249−59. (d) Chen, J.; Kuss-Petermann, M.; Wenger, O. S. *Chem. - Eur. J.* **2014**, *20*, 4098−104. (e) Chen, J.; Kuss-Petermann, M.; Wenger, O. S. *J. Phys. Chem. B* **2015**, *119*, 2263−73.

(11) Markle, T. F.; Rhile, I. J.; Mayer, J. M. *J. Am. Chem. Soc.* **2011**, *133*, 17341−17352. (b) Warren, J. J.; Menzeleev, A. R.; Kretchmer, J. S.; Miller, T. F.; Gray, H. B.; Mayer, J. M. *J. Phys. Chem. Lett.* **2013**, *4*, 519−523.

(12) Jovanovic, M. V.; Biehl, E. R. *J. Heterocycl. Chem.* **1983**, *20*, 1677−1680.

(13) (a) Driver, M. S.; Hartwig, J. F. *J. Am. Chem. Soc.* **1996**, *118*, 7217−7218. (b) Franz, A. W.; Popa, L. N.; Rominger, F.; Müller, T. J. J. *Org. Biomol. Chem.* **2009**, *7*, 469−475.

(14) Krämer, C. S.; Zimmermann, T. J.; Sailer, M.; Müller, T. J. J. *Synthesis* **2002**, *2002*, 1163−1170.

(15) Robichaud, J.; Oballa, R.; Prasit, P.; Falgueyret, J.-P.; Percival, M. D.; Wesolowski, G.; Rodan, S. B.; Kimmel, D.; Johnson, C.; Bryant, C.; Venkatraman, S.; Setti, E.; Mendonca, R.; Palmer, J. T. *J. Med. Chem.* **2003**, *46*, 3709−3727.

(16) (a) Kulkarni, A. P.; Wu, P.-T.; Kwon, T. W.; Jenekhe, S. A. *J. Phys. Chem. B* **2005**, *109*, 19584−94. (b) Franz, A. W.; Popa, L. N.; Rominger, F.; Müller, T. J. J. *Org. Biomol. Chem.* **2009**, *7*, 469−75.

(17) (a) Connelly, N. G.; Geiger, W. E. *Chem. Rev.* **1996**, *96*, 877. (b) Rhile, I. J.; Markle, T. F.; Nagao, H.; DiPasquale, A. G.; Lam, O. P.; Lockwood, M. A.; Rotter, K.; Mayer, J. M. *J. Am. Chem. Soc.* **2006**, *128*, 6075−6088. (c) Bandlish, B. K.; Shine, H. *J. Org. Chem.* **1977**, *42*, 561−563.

(18) Rosokha, S. V.; Kochi, J. K. *J. Am. Chem. Soc.* **2007**, *129*, 3683−3697.

(19) Evans, J. F.; Lenhard, J. R.; Blount, H. N. *J. Org. Chem.* **1977**, *42*, 983−988.

(20) Waidmann, C. R.; Miller, A. J. M.; Ng, C.-W. A.; Scheuermann, M. L.; Porter, T. R.; Tronic, T. A.; Mayer, J. M. *Energy Environ. Sci.* **2012**, *5*, 7771−7780.

(21) Manner, V. M.; Markle, T. F.; Freudenthal, J. H.; Roth, J. P.; Mayer, J. M. *Chem. Commun.* **2008**, 256−258.

(22) Kolthoff, I. M.; Chantooni, M. K.; Bhowmik, S. *Anal. Chem.* **1967**, *39*, 315−320.

(23) (a) Sackett, P. H.; Mayausky, J. S.; Smith, T.; Kalus, S.; McCreery, R. L. *J. Med. Chem.* **1981**, *24*, 1342−7. (b) Mayausky, J. S.; McCreery, R. L. *Anal. Chem.* **1983**, *55*, 308−312. (c) Zimová, N.; Němec, I.; Waisser, K. *Collect. Czech. Chem. Commun.* **1990**, *55*, 63−71. (d) Jovanovic, M. V.; Biehl, E. R.; De Meester, P.; Chu, S. S. C. *J. Heterocyclic Chem.* **1984**, *21*, 1425−1429.

(24) Frisch, M. J. et al. *Gaussian 09*, Revision A.1; Gaussian, Inc.: Wallingford CT, 2009. See Supporting Information for complete reference.

(25) Wilson, P. J.; Bradley, T. J.; Tozer, D. J. *J. Chem. Phys.* **2001**, *115*, 9233−9242.

(26) (a) Francl, M. M.; Pietro, W. J.; Hehre, W. J.; Binkley, J. S.; DeFrees, D. J.; Pople, J. A.; Gordon, M. S. *J. Chem. Phys.* **1982**, *77*, 3654−3665. (b) Clark, T.; Chandrasekhar, J.; Spitznagel, G. W.; Schleyer, P. v. R. *J. Comput. Chem.* **1983**, *4*, 294−301.

(27) (a) Clarke, D.; Gilbert, B. C.; Hanson, P. *J. Chem. Soc., Perkin Trans. 2* **1975**, 1078−1082. (b) Clarke, D.; Gilbert, B. C.; Hanson, P. *J. Chem. Soc., Perkin Trans. 2* **1976**, 114−214.

(28) Nikitin, K.; Müller-Bunz, H.; Ortin, Y.; Muldoon, J.; McGlinchey, M. J. *Org. Lett.* **2011**, *13*, 256−259.

(29) (a) Fronza, G.; Mondelli, R.; Scapini, G.; Ronsisvalle, G.; Vittorio, F. *J. Magn. Reson.* **1976**, *23*, 437−454. (b) Klein, C. L.; Conrad, J. M., III; Morris, S. A. *Acta Crystallogr., Sect. C: Cryst. Struct. Commun.* **1985**, *C41*, 1202−4.

DOI: 10.1021/acs.joc.5b01427
J. Org. Chem. 2015, 80, 8705−8712

(30) Marenich, A. V.; Cramer, C. J.; Truhlar, D. G. *J. Phys. Chem. B* **2009**, *113*, 6378−6396.
(31) (a) Osako, T.; Ohkubo, K.; Taki, M.; Tachi, Y.; Fukuzumi, S.; Itoh, S. *J. Am. Chem. Soc.* **2003**, *125*, 11027−1033. (b) Bordwell, F. G.; Cheng, J.-P. *J. Am. Chem. Soc.* **1991**, *113*, 1736−1743.
(32) Caroll, F. A. *Perspectives on Structure and Mechanism in Organic Chemistry*, 1st ed.; Brooks-Cole: Pacific Grove, 1998; p 357.
(33) Roth, J. P.; Lovell, S.; Mayer, J. M. *J. Am. Chem. Soc.* **2000**, *122*, 5486−98.
(34) Huynh, H. V.; Meyer, T. J. *Proc. Natl. Acad. Sci. U. S. A.* **2004**, *101*, 13138−41.
(35) Other examples are cited in Decornez, H.; Hammes-Schiffer, S. *J. Phys. Chem. A* **2000**, *104*, 9370−9384.
(36) Edwards, S. J.; Soudackov, A. V.; Hammes-Schiffer, S. *J. Phys. Chem. A* **2009**, *113*, 2117−26.
(37) Warren, J. J.; Mayer, J. M. *Proc. Natl. Acad. Sci. U. S. A.* **2010**, *107*, 5282−5287.
(38) (a) Marcus, R. A.; Sutin, N. *Biochim. Biophys. Acta, Rev. Bioenerg.* **1985**, *811*, 265−322. (b) Nelsen, S. F.; Blackstock, S. C.; Kim, Y. J. *J. Am. Chem. Soc.* **1987**, *109*, 677−682. (c) Chen, P.; Curry, M.; Meyer, T. J. *Inorg. Chem.* **1989**, *28*, 2271−80.
(39) Goldsmith, C. R.; Jonas, R. T.; Stack, T. D. P. *J. Am. Chem. Soc.* **2002**, *124*, 83−96.
(40) Zaytsev, A. V.; Anderson, R. J.; Bedernjak, A.; Groundwater, P. W.; Huang, Y.; Perry, J. D.; Orenga, S.; Roger-Dalbert, C.; James, A. *Org. Biomol. Chem.* **2008**, *6*, 682−692.
(41) Bell, F. A.; Ledwith, A.; Sherrington, D. C. *J. Chem. Soc. C* **1969**, 2719−2720.
(42) (a) Bandlish, B. K.; Shine, H. *J. Org. Chem.* **1977**, *42*, 561. (b) Eberson, L.; Larsson, B. *Acta Chem. Scand.* **1986**, *40*, 210. (c) Eberson, L.; Larsson, B. *Acta Chem. Scand.* **1987**, *41*, 367.
(43) Driver, M. S.; Hartwig, J. F. *J. Am. Chem. Soc.* **1996**, *118*, 7217−7218.
(44) Franz, A. W.; Popa, L. N.; Rominger, F.; Müller, T. J. J. *Org. Biomol. Chem.* **2009**, *7*, 469−475.
(45) Jovanovic, M. V.; Biehl, E. R. *J. Heterocycl. Chem.* **1983**, *20*, 1667−80.
(46) Gilman, H.; Ranck, R. O. *J. Org. Chem.* **1958**, *23*, 1903−1906.
(47) Kütt, A.; Leito, I.; Kaljurand, I.; Sooväli, L.; Vlasov, V. M.; Yagupolskii, L. M.; Koppel, I. A. *J. Org. Chem.* **2006**, *71*, 2829−38.
(48) Bordwell, F. G.; Zhang, X.-M. *J. Phys. Org. Chem.* **1995**, *8*, 529.
(49) Augustin-Nowacka, D.; Chmurzyński, L. *Anal. Chim. Acta* **1999**, *381*, 215−220.

DOI: 10.1021/acs.joc.5b01427
J. Org. Chem. 2015, 80, 8705−8712